

Characterization of Spinel Zinc Titanium Nitride Oxide as a Visible Light Driven Photocatalyst

Takashi Hisatomi,[1] Kentaro Teramura,[2] Jun Kubota,[1] and Kazunari Domen*[1]

[1]Department of Chemical System Engineering, School of Engineering, The University of Tokyo, 7-3-1 Hongo, Bunkyo-ku, Tokyo 113-8656

[2]Kyoto University Pioneering Research Unit for Next Generation, Kyoto University, Kyoto 615-8510

Received March 25, 2008; E-mail: domen@chemsys.t.u-tokyo.ac.jp

Physical properties of zinc titanium nitride oxides ($Zn_xTiO_yN_z$) were studied as a novel photocatalytic material with visible light activity. A series of $Zn_xTiO_yN_z$ having a spinel structure were obtained by nitriding an oxide precursor derived from a polymerized complex method under a high-temperature NH_3 flow for various durations. The $Zn_xTiO_yN_z$ spinel obtained was metastable because the Zn in the nitride oxide volatilized during the nitridation process. Both Zn and Ti cations of the $Zn_xTiO_yN_z$ spinel were essentially located in the same cation sites as the inverse spinel phase of Zn_2TiO_4; Zn species at the octahedral sites were volatilized in preference to those at tetrahedral sites. The bandgap energy of the $Zn_xTiO_yN_z$ spinel decreased as the amount of N species was increased, eventually stabilizing at 2.3 eV.

Photocatalytic water splitting has been widely studied as a potential large-scale technique to produce H_2 using solar energy. It is important to develop photocatalysts that can split water into H_2 and O_2 under visible light irradiation ($\lambda > 400$ nm) in order to utilize solar energy efficiently. However, to date, only a few such photocatalytic systems have been reported.[1–6] A key issue is the need to develop materials with the potential to use photons of longer wavelength.

It is generally thought that the crystal structure of a material plays a significant role in any potential photocatalytic ability. This is because the crystal structure is a determining factor of the energy band structures of a material and thus the light absorption and mobility of photoexcited carriers. Electrons and holes are generated within a photocatalytic material through light absorption at the initial stage of a photocatalytic reaction. Only some of these migrate to the surface of the material for successful photocatalysis; the rest immediately recombine. Taking these processes into account, it is reasonable to interpret photocatalytic properties in relation to a crystal structure of a photocatalyst material. For the water-splitting reaction, a series of compounds having perovskite,[7–9] wurtzite,[10–12] and pyrochlore[13,14] structures have been developed as photocatalysts.

Spinel compounds, derived from $MgAl_2O_4$, are interesting materials from the standpoint of photocatalyst development, as it seems that such compounds have suitable ionic arrangements for photocatalytic reactions. As shown in Figure 1, a spinel compound has both tetrahedral and octahedral sites for constituent cations, which makes it possible for cations having different site-preference to coexist stably in a single structure. In addition, it can countenance a number of cation and/or anion vacancies. It is thus possible for spinel compounds to possess a variety of compositions. Some spinel sulfides and oxides actually exhibit photocatalytic activity for H^+ reduction, with the aid of appropriate reducing reagents, or overall water splitting.[15,16] In spite of these stimulating features of the spinel structure, little was previously known of the photocatalytic properties of spinel nitride oxides.

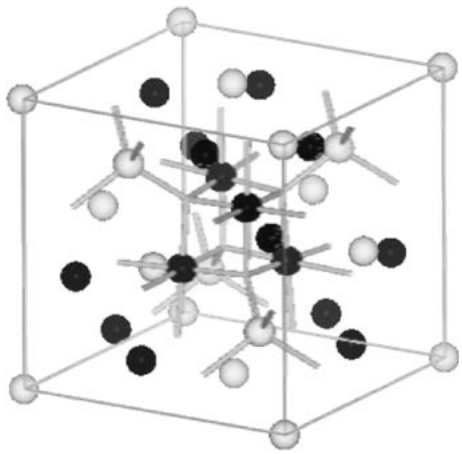

Figure 1. Crystal structure of a spinel compound. Anions are not described for simplicity. Gray and black spheres represent tetrahedrally and octahedrally coordinated cations, respectively. Some cation–anion bonds are shown as a guide.

Recently, zinc and titanium nitride oxides ("ZnTiON") that possessed spinel-like structures were developed through a colloidal sol–gel route by Grasset et al.[17,18] According to these authors, "ZnTiON" absorbs visible light and shows an absorption edge that red-shifts with increasing nitridation temperature or time. They concluded that anionic replacement of O^{2-} by N^{3-} was responsible for the visible light absorption by "ZnTiON." Berthebaud et al.[19] pointed out that on the basis of X-ray powder diffraction, the crystal structure of "ZnTiON" corresponded to that of a cation deficient spinel structure.

Published on the web December 12, 2008; doi:10.1246/bcsj.81.1647

The present authors employed "ZnTiON" spinels for photocatalytic applications and found that "ZnTiON" spinels prepared through a polymerized complex method functioned as a visible-light-driven photocatalyst that had potential to be active for water splitting.[20] Our preliminary work suggested that "ZnTiON" sustains spinel structure even though the chemical composition varies due to volatilization of Zn species and incorporation of N species during thermal treatment under an NH_3 flow. Since physicochemical properties such as crystallinity, chemical composition, and electronic states also influence photocatalytic performance, it is necessary to understand the nature of the "ZnTiON" spinel in depth so as to discuss and understand its photocatalytic properties. However, comprehensive properties of the "ZnTiON" spinels have yet to be clarified.

In this study, a series of zinc and titanium nitride oxides (expressed hereafter by $Zn_xTiO_yN_z$) were prepared by nitridation of an oxide precursor with different nitridation times. Crystal structures, chemical compositions, electronic states, and other properties of the $Zn_xTiO_yN_z$ spinels were investigated in association with the nitridation process and the photocatalytic activity.

Experimental

Preparation of $Zn_xTiO_yN_z$ Powder. $Zn_xTiO_yN_z$ powder was obtained by heating an oxide precursor prepared by a polymerized complex method under an NH_3 flow. Typically, 0.0412 mol of $Ti[OCH(CH_3)_2]_4$ (Kanto Chemical Co., Inc., 97.0%) was hydrolyzed with 110 mL of distilled water. 0.618 mol of citric acid (Wako Pure Chemical Industries, Ltd., 98.0%), 0.0824 mol of $Zn(NO_3)_2 \cdot 6H_2O$ (Kanto Chemical Co., Inc., 99.0%) and 2.5 mol of ethylene glycol (Kanto Chemical Co., Inc., 99.5%) were added to this suspension. The suspension became transparent during moderate heating with continuous stirring and it was transformed into a highly viscous gel in a day. The gel was carbonized at 673 K and then calcined at 823 K for 2 h in air, yielding a white oxide precursor. Some of the oxide precursor (1.50 g) was wrapped with silica wool and placed in a quartz tube. It was heated at the rate of 10 K min^{-1} by a tube furnace under 100 mL min^{-1} of NH_3 flow and held at 1023 K for up to 8 h. After the furnace was cooled to below 473 K under the NH_3 flow, the quartz tube was purged by N_2 and the product, $Zn_xTiO_yN_z$ powder, was collected. In this paper, nitridation time is expressed by the holding time at the target temperature, and samples were collected for a variety of holding times (Table 1).

Characterization. Crystalline phases of the products were analyzed by powder X-ray diffractometry (XRD; RINT-Ultima-III, Rigaku) using Cu Kα radiation with a source power of 40 kV and 40 mA. XRD patterns were collected at 2θ angles of 5–80° at a sweep rate of 2° min^{-1}. Diffuse reflectance spectra (DRS) were obtained using a UV–visible diffuse reflectance spectrometer (V-560, Jasco) and were converted from reflectance to absorbance on the basis of the Kubelka–Munk theory. Bandgap energies were evaluated based on eq 1 given direct or indirect allowed transition:[21,22]

$$(\alpha h\nu)^n = A(h\nu - E_g) \quad (1)$$

where, α is the absorption coefficient, $h\nu$ is the energy of the irradiating light, E_g is the bandgap energy of a semiconductor, and n is 2 for a direct allowable transition and 0.5 for an indirect allowable transition. Chemical compositions were determined by the molar ratio of Zn to Ti given by energy dispersive X-ray spectroscopy (EDS; Emax-7000, Horiba) and absolute weight percentage of O and N measured by an oxygen–nitrogen analyzer (EMGA-620W, Horiba), where it was assumed that the sum of weight fractions of Zn, Ti, O, and N was equal to unity. Surface states were characterized by X-ray photoelectron spectroscopy (XPS; JPS-90SX, Jeol) using Mg Kα radiation. All binding energies were corrected using, as a reference, the C1s peak (285.0 eV). X-ray absorption fine structure (XAFS) of the Zn-K edge and Ti-K edge were measured in the BL9A beamline of the Photon Factory (High Energy Accelerator Research Organization, Tsukuba, Japan) using a ring energy of 2.5 GeV and stored current from 450 to 280 mA (Proposal No. 2007G624). Nitrogen adsorption measurements were carried out at 77 K using a BELSORP-mini (BEL Japan). Specific surface areas were calculated based on the Brunauer–Emmett–Teller (BET) method. Powder morphologies were observed using field-emission scanning electron microscopy (SEM; S-4700, Hitachi). Thermogravimetric and differential thermal analyses (TG-DTA) was performed using a Thermo plus II (Rigaku), where 15.3 mg of the $Zn_xTiO_yN_z$ nitrided for 4 h was placed on an alumina pan and heated up to 1673 K at a rate of 10 K min^{-1} under 100 mL min^{-1} of air flow.

Table 1. Chemical Compositions and Bandgap Energies of $Zn_xTiO_yN_z$ Prepared with Various Nitridation Times

Entry	t/h	Chemical composition[a)]	Nitrogen-to-anion ratio[b)] (at/at)	$E_{g,ind}$/eV
A	oxide	$Zn_{2.0}TiO_{3.9}$	0.00	3.1
B	0	$Zn_{1.9}TiO_{3.5}N_{0.2}$	0.05	2.7
C	2	$Zn_{1.6}TiO_{3.0}N_{0.3}$	0.10	2.4
D	3	$Zn_{1.4}TiO_{2.8}N_{0.4}$	0.12	2.4
E	4	$Zn_{1.4}TiO_{2.8}N_{0.4}$	0.12	2.3
F	5	$Zn_{1.2}TiO_{2.6}N_{0.4}$	0.13	2.3
G	6	$Zn_{1.1}TiO_{2.5}N_{0.4}$	0.15	2.3
H	8	$Zn_{1.0}TiO_{2.4}N_{0.4}$	0.15	2.3

a) The ratio of Zn to Ti and the absolute amount of O and N was determined by EDS and oxygen–nitrogen analysis respectively, given that the sum of weight percentage of Zn, Ti, O, and N was unity. b) N/(N + O) by atom number.

Photocatalytic Reaction. Photooxidation of H_2O to O_2 and photoreduction of H^+ to H_2 were performed separately in the presence of an electron acceptor (Ag^+) and donor (methanol) in a top-irradiation Pyrex reaction vessel connected to a closed gas circulation and evacuation system. For the O_2 evolution reaction, 0.20 g of $Zn_xTiO_yN_z$ was suspended in 200 mL of 10 mM (=mmol dm^{-3}) $AgNO_3$ aqueous solution containing 0.20 g of La_2O_3 powder, which was added to prevent pH decrease during the reaction. For the H_2 evolution reaction, $Zn_xTiO_yN_z$ was modified with 1.0 wt % Pt prior to the reaction. The Pt was loaded by impregnation from an $H_2[PtCl_6]$ aqueous solution followed by hydrogen reduction treatment at 473 K for 2 h. The Pt-loaded $Zn_xTiO_yN_z$ (0.20 g) was suspended in 200 mL of 10 vol % methanol aqueous solution. After this initial preparation, each reaction vessel was evacuated several times to completely remove air from the reaction system before irradiation proceeded. The light source for irradiation was a 300-W Xe lamp equipped with cutoff filter ($\lambda > 420$ nm). Evolved gases were analyzed by a gas chromatograph (GC-8A, TCD, Ar carrier, MS5A column).

The apparent quantum efficiency (Φ), which was evaluated based on the number of incident photons, was calculated using eq 2:

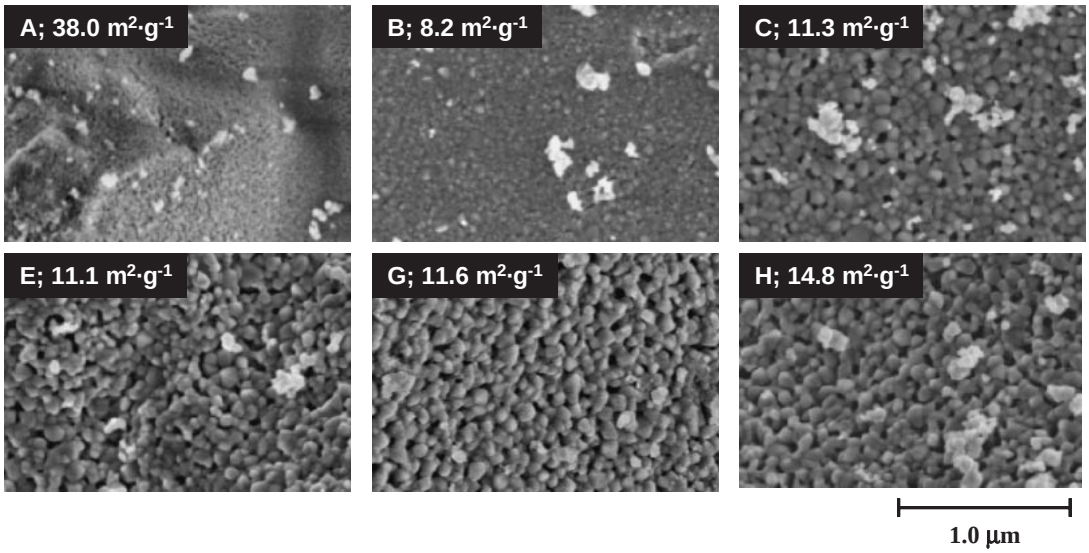

Figure 2. SEM images of (A) the oxide precursor and (B–H) $Zn_xTiO_yN_z$ nitrided for (B) 0, (C) 2, (E) 4, (G) 6, and (H) 8 h. Specific surface areas measured by the BET method are also indicated.

$$\Phi = (AR/I) \quad (2)$$

where A, R, and I are coefficients based on the reactions (for H_2 evolution reaction, 1, and for O_2 evolution reaction, 4),[23] the H_2 or O_2 evolution rate and the number of incident photons per unit time, respectively. The number of incident photons were measured to be $\approx 1.7 \times 10^{22}$ photon h^{-1} at 420–560 nm using a Si photodiode and two cutoff filters ($\lambda > 420$ nm and $\lambda > 560$ nm).

Results and Discussion

Morphology Observation. Figure 2 shows SEM images of the oxide precursor and the $Zn_xTiO_yN_z$ obtained at 1023 K with various nitridation times. Specific surface areas determined by the BET method are also indicated on the images. The oxide precursor formed micron-size secondary particles consisting of aggregates of primary particles that were smaller than 50 nm. This is characteristic morphology of oxides prepared at low temperature using the polymerized complex method. The primary particle size grew to 50–100 nm while the specific surface area was decreased as a result of nitridation at 1023 K for 2 h. The primary particle growth seemed to continue with further nitridation. However, locating primary particles definitely larger than 100 nm, even after nitridation over 8 h, was difficult. Gradual increase in the specific surface area in accordance with nitridation also suggests that sintering of the $Zn_xTiO_yN_z$ was negligible. One possible reason for these results is continuous volatilization of Zn during the nitridation treatment. It became difficult to sustain the spinel structure of $Zn_xTiO_yN_z$ as the nitridation reaction proceeded because of the lack of Zn species. As a result, the $Zn_xTiO_yN_z$ spinel crystals hardly grew at 1023 K under a NH_3 flow, while the secondary particles of $Zn_xTiO_yN_z$ maintained an interparticle macropore. This feature is different from $(Ga_{1-x}Zn_x)(N_{1-x}O_x)$ where solid solutions of a wurtzite structure formed.[10]

Bulk Structure Analysis. Figure 3 shows the XRD patterns of the oxide precursor and the $Zn_xTiO_yN_z$ prepared at 1023 K with various nitridation times. The spinel phase of

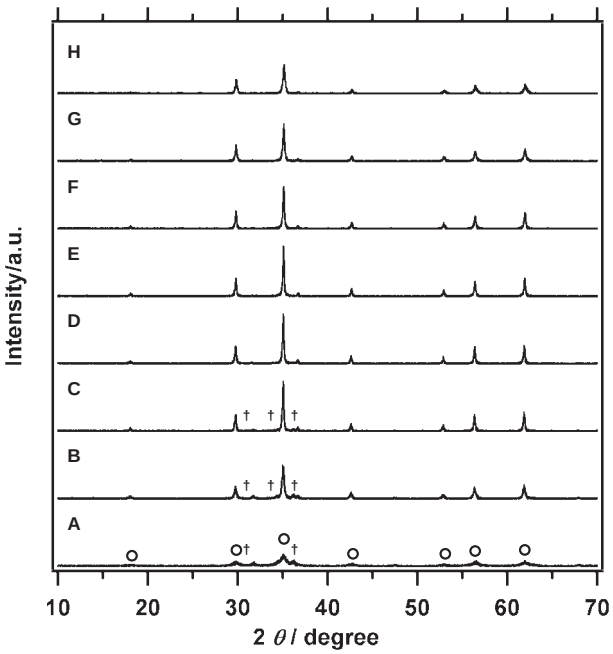

Figure 3. XRD patterns of (A) the oxide precursor and (B–H) $Zn_xTiO_yN_z$ nitrided for (B) 0, (C) 2, (D) 3, (E) 4, (F) 5, (G) 6, and (H) 8 h. ○: Zn_2TiO_4; †: ZnO.

Zn_2TiO_4 and the wurtzite phase of ZnO were observed in the diffraction pattern of the oxide precursor, although the intensities were weak because of insufficient crystallization. Taking the chemical composition of the oxide precursor into account, residual Ti species should be contained as amorphous phases. The spinel phase became dominant while the ZnO phase disappeared with an increase in nitridation time. Nitridation for 3–4 h yielded a XRD-pure $Zn_xTiO_yN_z$ spinel. The diffraction peaks attributed to the spinel phase were prominent over the nitridation process. However, nitridation for more than 4 h diminished the diffraction peak intensities of the $Zn_xTiO_yN_z$ spinel, indicating collapse of the spinel structure.

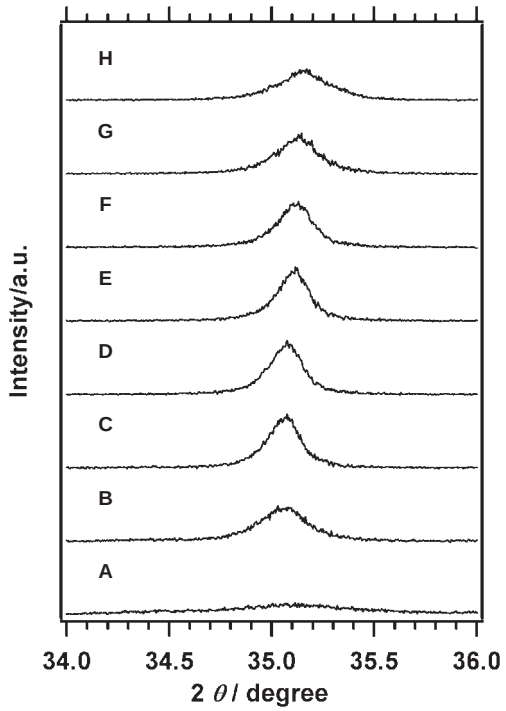

Figure 4. Magnified diffraction peak corresponding to (311) of Zn_2TiO_4 spinel structure. (A) the oxide precursor and (B–H) $Zn_xTiO_yN_z$ nitrided for (B) 0, (C) 2, (D) 3, (E) 4, (F) 5, (G) 6, and (H) 8 h.

As is described later, it is suggested that this instability of the spinel phase of $Zn_xTiO_yN_z$ is due to continuous volatilization of Zn.

The (311) diffraction peaks of the spinel structure shifted toward the higher angle in accordance with nitriding as shown in Figure 4, indicating shrinkage of the $Zn_xTiO_yN_z$ spinel lattice during the nitridation. If an oxide is converted into a nitride without its crystal structure changing, its unit cell should be expanded since the ionic radius of N^{3-} anion is larger than that of O^{2-}.[24] It is thus conjectured that cation and/or anion defects are produced in $Zn_xTiO_yN_z$ spinel during the nitridation reaction. Considering the fact that the ionic radius of Ti^{4+} is smaller than that of Zn^{2+}, it is possible that Zn^{2+} cations are partially replaced by Ti^{4+} cations at the octahedral sites of the spinel structure. Indeed, there exists a $Zn_2Ti_3O_8$ structure in which Zn^{2+} cations are excluded entirely from octahedral sites by Ti^{4+} cations.[25]

Local Structure Analysis. XAFS measurements were carried out in order to determine the local structure around Zn and Ti in $Zn_xTiO_yN_z$. Figure 5 shows the X-ray absorption near-edge structures (XANES) of the Zn-K and Ti-K edge for $Zn_xTiO_yN_z$ nitrided for 4 h. The spectra for Zn foil, ZnO, $ZnTiO_3$, Zn_2TiO_4, TiN, and TiO_2 (rutile) are also shown as references. The XANES spectrum of Zn-K edge for the $Zn_xTiO_yN_z$ was identical to that of the Zn_2TiO_4 spinel, while it was obviously different from that of the other reference spectra. In addition, no difference in edge position was observed between the $Zn_xTiO_yN_z$ and Zn_2TiO_4. These results indicate that the valence state and the local structure of Zn species in the $Zn_xTiO_yN_z$ is essentially the same as that for the Zn_2TiO_4. Furthermore, no significant pre-edge peaks were found in any

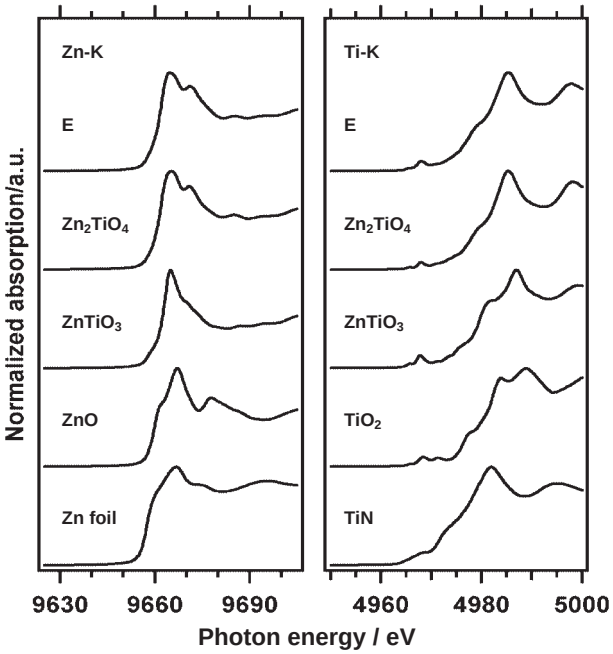

Figure 5. Zn-K and Ti-K edge XANES spectra for (E) $Zn_xTiO_yN_z$ nitrided for 4 h. Zn foil, ZnO, $ZnTiO_3$, Zn_2TiO_4, TiN, and TiO_2 (rutile) are shown as references.

of the Zn-K edge XANES spectra, reflecting the fact that Zn species does not have any vacant d orbitals.[26]

The XANES spectrum of the Ti-K edge for $Zn_xTiO_yN_z$ also corresponded to that of the Zn_2TiO_4 spinel rather than any other reference material. No significant change was observed in the spectral shape or the position of the absorption edge between the $Zn_xTiO_yN_z$ and Zn_2TiO_4, again indicating that Ti species in the $Zn_xTiO_yN_z$ maintained the local structure and the valence state of Ti in Zn_2TiO_4. Note that the Ti^{4+} species in the $Zn_xTiO_yN_z$ were hardly reduced after the nitridation treatment although Ti^{4+} species in common Ti oxides, for instance TiO_2, were reduced easily under a high-temperature NH_3 flow.[27] The unusual stability of Ti^{4+} species in $Zn_xTiO_yN_z$ is confirmed in a series of DRS of $Zn_xTiO_yN_z$ shown later. The Ti-K edge XANES spectra for $Zn_xTiO_yN_z$ did show a pre-edge peak at 4968 eV, although its intensity was relatively low. It is known that pre-edge peak intensity of Ti-K edge XANES is dependent on the coordination number of Ti species[28] and, in general, that six-coordinated Ti species show smaller pre-edge peaks than four-coordinated ones. Therefore, it is believed that the Ti species in $Zn_xTiO_yN_z$ are located at octahedral sites of the spinel structure.

Figure 6 shows the Fourier transforms of k^3-weighted EXAFS spectra of the Zn-K and Ti-K edges for $Zn_xTiO_yN_z$ obtained by nitridation over various durations. Radial structure functions for Zn_2TiO_4 are also indicated for comparison. Three characteristic peaks were observed at 1.6, 2.6, and 3.1 Å in the radial structure function of Zn-K edge for Zn_2TiO_4. A crystal structure analysis of Zn_2TiO_4 revealed that the lengths of Zn–O bonds, Zn_{octa}–M_{octa} bonds, and Zn–X bonds were 2.0, 3.0, and 3.5–3.7 Å, respectively, where M = Zn or Ti, X = Zn, Ti, or O, and octa refers to octahedral sites of a spinel structure, respectively.[29] The peak positions of the observed radial structure function of Zn were slightly shorter than the

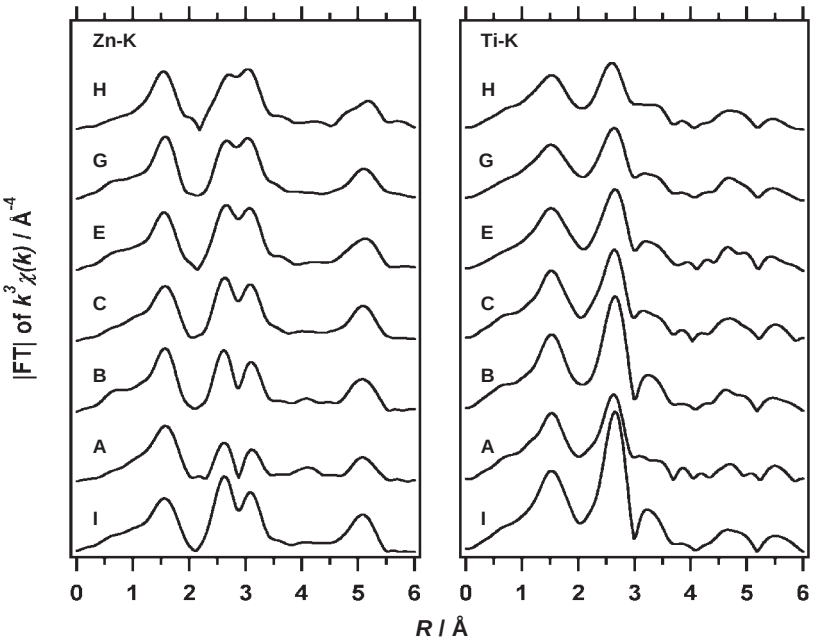

Figure 6. Fourier transforms of k^3-weighted Zn-K and Ti-K edge EXAFS spectra for (A) the oxide precursor and $Zn_xTiO_yN_z$ nitrided for (B) 0, (C) 2, (E) 4, (G) 6, and (H) 8 h. Data for Zn_2TiO_4 (I) is shown for reference.

crystallographic structural data due to phase shift. Accordingly, the peaks at 1.6, 2.6, and 3.1 Å were attributed to Zn–O bonds, Zn_{octa}–M_{octa} bonds and Zn–X bonds of the $Zn_xTiO_yN_z$ spinel structure, respectively.

The peak at 2.6 Å, which was characteristic of octahedrally coordinated Zn species, became smaller than that at 3.1 Å with the progress of nitridation although it was prominent at the beginning of nitridation. Navrotsky and Kleppa[30] found in thermodynamic studies of spinels that Zn species located at octahedral sites were less stable than those located at tetrahedral sites. Considering the instability of six-coordinated Zn species, it is reasonable to suggest that Zn species at the octahedral sites of $Zn_xTiO_yN_z$ spinel volatilized in preference to those at the tetrahedral sites. In order to quantitatively justify this proposal, curve fitting and simulation analyses of EXAFS are currently being undertaken.

In the radial structure function of the Ti-K edge for Zn_2TiO_4, three peaks were observed at 1.6, 2.6, and 3.2 Å, although the peak at 3.2 Å was almost absent unlike the radial structure function of Zn-K edge. Based on comparison with crystallographic structural data,[29] these peaks were attributed to Ti–O bonds, Ti_{octa}–M_{octa} bonds, and Ti–X bonds, respectively. The indistinct peak for the Ti–X bonds is probably because the Ti species are not located at tetrahedral sites in the Zn_2TiO_4 spinel structure and thus contribution to the peak is limited. Confirmation that the Ti species essentially exist at the octahedral site of the spinel structure is shown by the fact that, over the nitridation, the radial structure function of Ti-K edge for $Zn_xTiO_yN_z$ did not show characteristic changes in the peak positions.

Surface State Analysis. Figure 7 shows the $2p_{3/2}$ XPS spectra and $L_3M_{4,5}M_{4,5}$ Auger electron spectra of Zn for Zn_2TiO_4 and the prepared $Zn_xTiO_yN_z$ samples. The $2p_{3/2}$ spectra could not be sufficiently fitted using a single Gaussian–Lorentzian curve, suggesting that several kinds of Zn species existed on

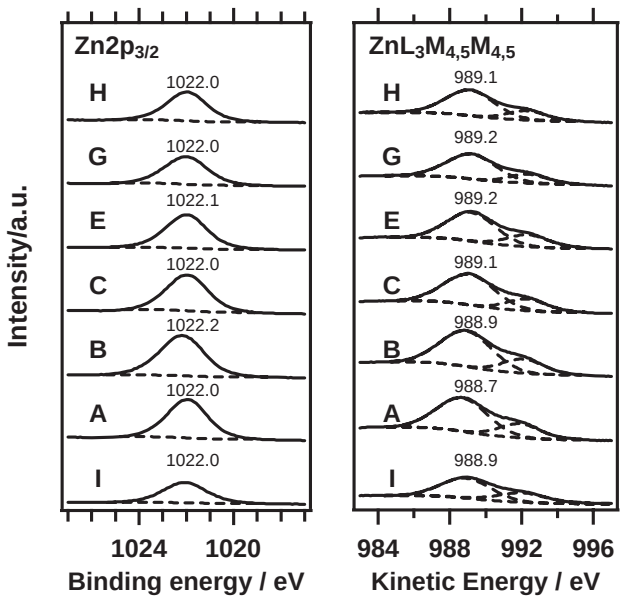

Figure 7. XPS spectra of $Zn2p_{3/2}$ and Auger electron spectra of $ZnL_3M_{4,5}M_{4,5}$ for (A) the oxide precursor and (B–H) $Zn_xTiO_yN_z$ nitrided for (B) 0, (C) 2, (E) 4, (G) 6, and (H) 8 h and (I) Zn_2TiO_4.

the surface of the nitride oxides. It is known that Ti species in spinel oxides such as $LiFeTiO_4$, $LiMnTiO_4$, and $LiCrTiO_4$ are located both at tetrahedral and octahedral sites in the spinel structure. Arillo et al.[31] reported that Ti $2p_{3/2}$ peaks for these spinel oxides were split into two peaks depending on the site occupancy: a peak deriving from tetrahedral sites appears at higher energy, and from octahedral sites at lower energy. Zn species in Zn_2TiO_4 and $Zn_xTiO_yN_z$ are also located both at tetrahedral and octahedral sites of the spinel structure. Therefore, it is reasonable that single curve fitting could not be performed.

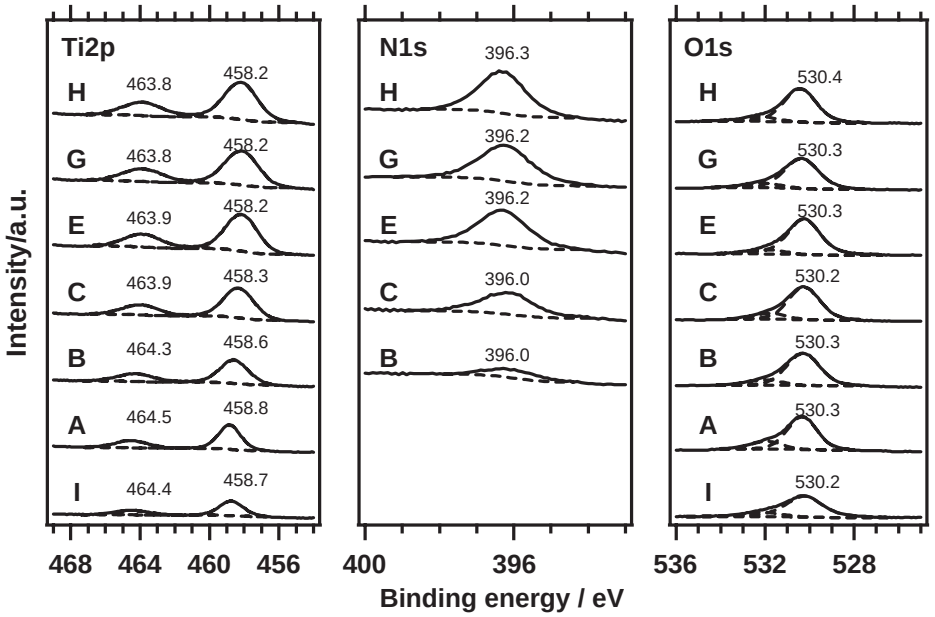

Figure 8. XPS spectra of (A) the oxide precursor and (B–H) $Zn_xTiO_yN_z$ nitrided for (B) 0, (C) 2, (E) 4, (G) 6, and (H) 8 h and (I) Zn_2TiO_4.

It is generally difficult to distinguish valence states of Zn species based on chemical shift of XPS, for the $2p_{3/2}$ chemical shift is insensitive to the chemical environment of Zn species.[32] Indeed, the XPS spectra shown in Figure 6 did not exhibit significant changes in binding energy.

In order to investigate the valence state of the Zn species in detail, $L_3M_{3,4}M_{4,5}$ Auger electron spectra were studied. Auger lines for the oxide precursor, Zn_2TiO_4 and $Zn_xTiO_yN_z$ were separated into two main peaks, which were attributed to *L–S* coupling.[33] The Auger peak shifted toward higher kinetic energy from 988.7 to 989.1–989.2 eV during the nitridation treatment. The kinetic energy for the $Zn_xTiO_yN_z$ was 0.2–0.3 eV larger than that for Zn_2TiO_4. Moreover, modified Auger parameters, reckoned by adding the binding energy of the Zn $2p_{3/2}$ and kinetic energy of Zn $L_3M_{4,5}M_{4,5}$, increased from 2010.7 to 2011.0–2011.2 eV. An increase in Auger electron kinetic energy results from an increase in valence electron density,[34] while a less polarizable compound gives a lower modified Auger parameter.[35] Therefore, these changes are probably associated with nitrogen incorporation; that is, Zn–N bond formation in place of Zn–O in $Zn_xTiO_yN_z$. The smaller shifts observed between $Zn_xTiO_yN_z$ and Zn_2TiO_4 ($\approx$0.2 eV) compared with those between ZnO and Zn_3N_2 ($\approx$2.1 eV)[34] are reasonable because the amount of nitrogen incorporated in the spinel lattice was small as well.

Figure 8 depicts the Ti 2p, N 1s, and O 1s XPS spectra for Zn_2TiO_4 and prepared $Zn_xTiO_yN_z$ samples. The binding energy of the Ti 2p orbital became smaller with the progress of nitridation, and eventually decreased by approximately 0.6 eV. This chemical shift resulted because more electronegative Ti–N bonds were partially substituted for less electronegative Ti–O bonds. Full width at half maximum of Ti 2p XPS spectra gradually increased (that is, the peaks broadened) in accordance with nitriding duration. At the same time, the accuracy of curve fitting with a single Gaussian–Lorentzian deteriorated, suggesting production of another Ti species. Indeed, based on the result of UV–visible DRS shown later, the Ti^{4+} species in $Zn_xTiO_yN_z$ was in part reduced to Ti^{3+}. The N 1s peaks became stronger as the nitridation time became longer. In addition, the peak position shifted toward higher binding energy. Shinn and Tsang[36] reported on surface N species observed in XPS: an N 1s peak observed around 397.5 eV is attributed to α-N_2, which originates from a N_2 molecule adsorbed on a surface with both nitrogen atoms coordinated. Another peak around 396.0 eV comes from β-N, which is atomic N species that are substituted for lattice oxygen. The other peak observed at 400–405 eV is attributed to γ-N_2, derived from a N_2 molecule chemisorbed on a surface by a single nitrogen atom. Considering these N species, the N 1s peak that emerged at 396.0–396.3 eV by nitridation of the oxide precursor was attributable to N^{3-} anions incorporated into the $Zn_xTiO_yN_z$ spinel lattice. The O 1s peaks were separated into two peaks of surface hydroxy groups at higher energy and lattice oxygen at lower energy.[34] No significant chemical shift was observed in O 1s spectra regardless of nitridation time.

Chemical Composition. The chemical compositions of $Zn_xTiO_yN_z$ are shown in Table 1. They are normalized by Ti content, which is not volatile over the nitridation treatment. The Zn content of $Zn_xTiO_yN_z$ was decreased continuously with the increase in nitridation time. This is because Zn^{2+} cations in $Zn_xTiO_yN_z$ were reduced to metallic Zn and volatilized under the nitridation conditions. Considering the fact that the boiling point of Zn is as low as 1180 K, vapor pressure of Zn is not negligible at that temperature. Decrease of volatile components such as Zn and alkaline metals is commonly observed during preparation of nitride oxides using a high-temperature NH_3 flow.[4,10,37]

The nitrogen-to-anion ratio of $Zn_xTiO_yN_z$ increased over the nitridation process as shown in Table 1, while the oxygen-to-anion ratio decreased. This result reflects the progress of nitridation with increase in nitridation time. Although nitridation for more than 4 h slightly increased the nitrogen-to-anion ratio,

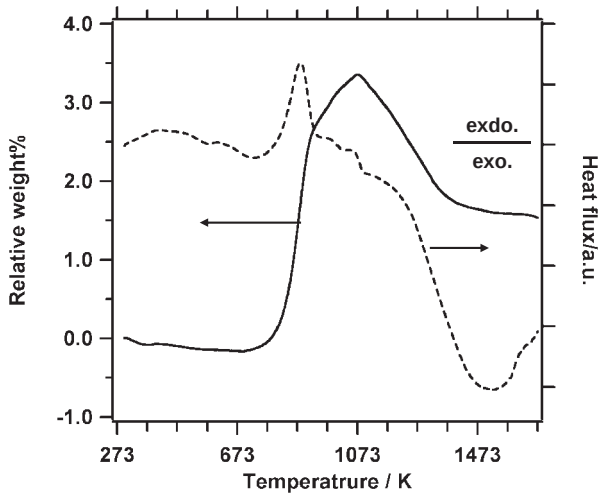

Figure 9. TG-DTA curve of $Zn_xTiO_yN_z$ nitrided for 4 h. Solid line: TG; dotted line: DTA.

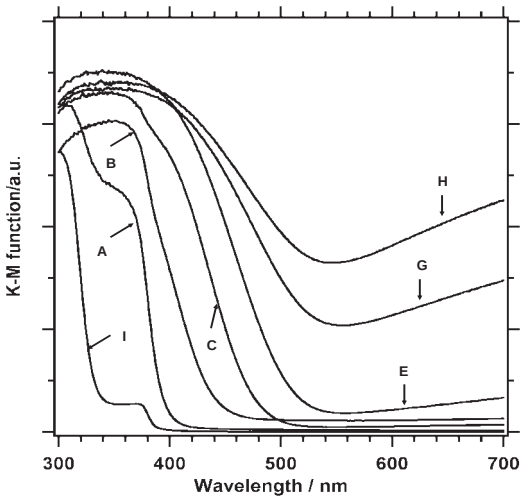

Figure 10. UV–visible diffuse reflectance spectra of (A) the oxide precursor and (B–H) $Zn_xTiO_yN_z$ nitrided for (B) 0, (C) 2, (E) 4, (G) 6, and (H) 8 h and (I) Zn_2TiO_4.

crystallinity of $Zn_xTiO_yN_z$ spinel deteriorated at the same time. Therefore, the nitrogen-to-anion ratio of the spinel phase of $Zn_xTiO_yN_z$ seemed to be 0.12 at most. This is somewhat lower than that of other photocatalytically active nitride oxides such as TaON, $BaTaO_2N$, and $(Ga_{1-x}Zn_x)(N_{1-x}O_x)$, and comparable with Berthebaud's reports on "$Zn_xTi_xO_{4-3y}N_{2y}$."[19] Taking the crystallographic stability into account, a certain amount of Zn is required in order to sustain the spinel structure of Zn_2TiO_4, yet nitridation under a NH_3 flow is necessarily accompanied by evaporation of Zn. This conflict makes it difficult to increase the nitrogen-to-anion ratio of $Zn_xTiO_yN_z$ spinel.

Thermal Stability. Figure 9 presents the TG-DTA curve of the $Zn_xTiO_yN_z$ nitrided for 4 h (product E in Table 1; $Zn_{1.4}TiO_{2.8}N_{0.4}$). A significant weight increase started at 690 K in the TGA curve and was accompanied by an exothermic signal peaking at 883 K in the DTA curve. This weight gain with exothermic reaction is attributed to oxidation of $Zn_xTiO_yN_z$. Note that the relative weight peaked when the reaction temperature was 1074 K, decreasing with considerable endothermic reaction afterwards. Le Gendre et al.[38] attributes this kind of intermediate weight gain for nitride oxides to nitrogen retention. This mechanism is also responsible for the intermediate weight gain in the case of $Zn_xTiO_yN_z$. The subsequent weight decrease accompanied by endothermic reaction is attributable to desorption of N_2. The net weight gain after the temperature reached 1673 K was 1.5% of the initial mass. Assuming that the valence state of the metal cation remains constant, oxidation of a metal nitride oxide is expressed by eq 3:

$$MO_xN_y + \frac{3}{4}yO_2 \rightarrow MO_{x+\frac{3}{2}y} + \frac{y}{2}N_2 \quad (3)$$

The weight gain thus corresponds to the composition of $Zn_{1.4}TiO_{2.9}N_{0.3}$, which accords with the result of oxygen–nitrogen analysis, $Zn_{1.4}TiO_{2.8}N_{0.4}$.

Optical Properties. Figure 10 shows DRS of the $Zn_xTiO_yN_z$ and Zn_2TiO_4 prepared by solid-state reaction. The DRS of Zn_2TiO_4 showed two absorption edges at 390 and 340 nm. The absorption edge at 390 nm agreed well with that of ZnO. The corresponding absorbance decreased after dilute HCl solution treatment, although the absorption below 340 nm did not change. Therefore, the absorption edges were attributed to residual ZnO and Zn_2TiO_4, respectively.

The DRS of the oxide precursor showed the absorption edges of both Zn_2TiO_4 and ZnO. Additionally, it is possible that light absorption by amorphous TiO_2 was observed at wavelengths shorter than 390 nm. After nitridation of the oxide precursor, the products, $Zn_xTiO_yN_z$, absorbed visible light ($\lambda > 400$ nm) although the oxide precursor did not. Absorption of visible light increased as the nitridation proceeded and the apparent absorption edge estimated from the onset of light absorption shifted toward longer wavelength. These features of nitride oxides result from the replacement of oxygen anions by nitrogen anions, raising the valence band top potential.[39–41] Although Zn species sometimes show considerable influences on narrowing the bandgap of oxide and nitride oxides, as is reported on $ZnGa_2O_4$,[16] $(Ga_{1-x}Zn_x)(N_{1-x}O_x)$[10] and $(Zn_{1+x}Ge)(N_2O_x)$,[4] it is not clear yet that those in $Zn_xTiO_yN_z$ have effects on the bandgap energy.

The apparent absorption edge reached 540 nm in 4 h. However, broad absorption emerged at longer wavelengths occurred afterward. This kind of light absorption is frequently observed in materials that contain an easily reducible element, like $LaTiO_2N$,[23] $TiN_xO_yF_z$,[42] and $ANbO_2N$ (A = Ca, Sr, and Ba),[43] and is attributed to intraband transition of d electrons that arose from reduced metal cations. Therefore, it is considered that the later broad light absorption by $Zn_xTiO_yN_z$, which was not evident at the beginning of the nitridation, appeared because the Ti species was partially reduced as the result of excess nitridation reaction. This resistivity of Ti^{4+} species in $Zn_xTiO_yN_z$ to the reductive atmosphere is presumably attributable to the influence of ZnO, for the Ti^{4+} species were less reduced during nitridation treatment when the Zn-to-Ti ratio was larger, be it of the oxide precursors or products. By contrast, when TiO_2 was exposed to a high-temperature NH_3 flow, it was converted into a bluish-black compound, indicating reduction of the Ti^{4+} species. From these observations, it is suggested that ZnO species suppressed reduction of the Ti^{4+} species in $Zn_xTiO_yN_z$ during the nitriding.

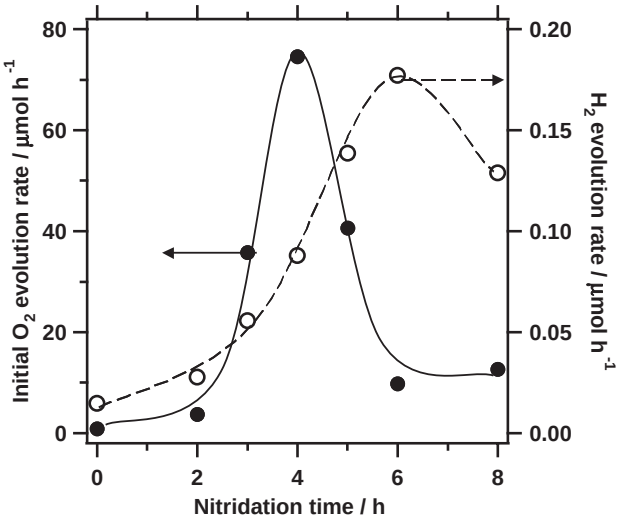

Figure 11. Dependence of the photocatalytic activity of $Zn_xTiO_yN_z$ for the O_2 and H_2 evolution reaction on nitridation time. The reaction conditions are described in the experimental section.

The bandgap energies of the prepared samples were estimated using eq 1. The bandgap energies became larger than the apparent bandgap energies when direct transition was assumed for light absorption by the products. By contrast, the assumption of indirect transition showed good accordance with the apparent bandgap energies, suggesting that $Zn_xTiO_yN_z$ is an indirect transition semiconductor. Given indirect transition, the bandgap energies of $Zn_xTiO_yN_z$ obtained by nitridation for various times are summarized in Table 1. The bandgap energy of $Zn_xTiO_yN_z$ decreased with increase in nitridation time, reaching 2.3 eV after 4 h nitridation. In the previous study, $Zn_xTiO_yN_z$ nitrided for 4 h showed photocatalytic activity under light irradiation up to 540–560 nm,[20] indicating that bandgap energy of the $Zn_xTiO_yN_z$ was equivalent to 2.3–2.2 eV on the basis of the photocatalytic activity. Consequently, the bandgap energy of $Zn_xTiO_yN_z$ was estimated with considerable accuracy of 0.1 eV on the assumption of indirect transition. The bandgap energy stabilized at 2.3 eV after nitridation for 4 h. This is probably because the ratio of nitrogen to the total anions did not change significantly after that time.

Photocatalytic Activity. $Zn_xTiO_yN_z$ is a photocatalyst active for H_2 and O_2 evolution under visible irradiation ($\lambda > 420$ nm) in the presence of sacrificial reagents.[20] The effect of nitridation time on the photocatalytic activity of $Zn_xTiO_yN_z$ was assayed to investigate the physicochemical factors influencing their performance. Figure 11 shows the relationship between the photocatalytic activity of $Zn_xTiO_yN_z$ and nitridation time, where O_2 evolution and H_2 evolution reactions were carried out separately in the presence of sacrificial reagents under visible light irradiation ($\lambda > 420$ nm).

O_2 evolution activity of $Zn_xTiO_yN_z$ depended significantly on the nitridation time. It increased with nitridation time to a peak at 4 h with activity of 75 μmol h^{-1}, which corresponded to 1.0% of the apparent quantum efficiency, and dropped rapidly afterward. At the beginning of the reaction, N_2 was sometimes evolved,[20] although the total amount was small (<8 μmol) and independent of the nitridation time and N content in $Zn_xTiO_yN_z$. In contrast, it depended on the O_2 evolution activity, suggesting that the transiently-evolved N_2 derived from photooxidation of N species existing on surface of $Zn_xTiO_yN_z$. Improvement in crystallinity and purity of the spinel phase are probably responsible for the increase in O_2 evolution activity by moderate nitridation (Figures 3B–3E), because it is generally accepted that lattice defects and surface impurities act as recombination centers for photoexcited electrons and holes. Increase in visible light absorption by incorporation of N^{3-} possibly contributed to the acceleration of the photocatalytic reaction as well (Figure 10 and Table 1, Entries B–E). By contrast, collapse of the spinel phase and partial reduction of Ti^{4+} species as the result of excess nitridation had negative effects on the photocatalytic activity (Figure 3 and Figures 10E–10H). The $Zn_xTiO_yN_z$ nitrided for 4 h displayed the highest O_2 evolution activity probably owing to the best matching of these incompatible effects of nitridation. Consequently, the photocatalytic activity of $Zn_xTiO_yN_z$ follows a generally accepted rule: high crystallinity and purity are essential to maximize performance of a photocatalyst, while a photocatalyst having metal cations with partially filled d orbitals, which can also act as recombination centers of photoexcited electrons and holes, shows reduced activity. For some photocatalytic systems, the O_2 evolution activity from an aqueous $AgNO_3$ solution is affected by the specific surface area of the photocatalyst,[44] or more precisely the adsorption capacity of the Ag^+ cation.[45] However, for $Zn_xTiO_yN_z$, there is no clear relationship between the O_2 evolution activity and the specific surface area, indicating that the specific surface area of $Zn_xTiO_yN_z$ has a minor effect on the photocatalytic activity.

H_2 evolution activity of $Zn_xTiO_yN_z$ also depended on the nitridation time, which can be explained in a similar way to O_2 evolution activity. The optimum nitridation time for H_2 evolution reaction was longer than that for O_2 evolution, and thus corresponded to when the Ti species in $Zn_xTiO_yN_z$ were partially reduced. The preference of partially reduced Ti species in the H_2 evolution reaction is possibly associated with improved conductivity of the photocatalyst in analogy with H_2-doping on oxides.[46] Actually however, photocatalytic activity is affected by adsorption properties, band structure, carrier lifetime, and other properties specific to each photocatalyst. A comprehensive clarification of the photocatalysis by $Zn_xTiO_yN_z$ is now under discussion. The apparent quantum efficiency for H_2 evolution reaction was less than 0.01% and practically negligible. Therefore, in order to achieve overall water splitting reaction by photoexcited electrons using this nitride oxide, it is important to somehow enhance the H^+ reduction reaction. Modification of a photocatalyst with proper cocatalysts often serves quite effectively for such purposes. Photocatalytic activity of $Zn_xTiO_yN_z$ was, however, almost diminished after calcination at 573 K for 1 h in the atmosphere although $Zn_xTiO_yN_z$ did not display significant change in the TG-DTA curve up to 690 K. This result indicates a difficulty in supporting appropriate cocatalysts on $Zn_xTiO_yN_z$ by any impregnation method that is accompanied by thermal treatment. Cocatalyst loading by a photodeposition technique did not work efficiently on $Zn_xTiO_yN_z$ either, similar to the case of TaON.[47] These difficulties reinforce the necessity of further

examination and improvement of photocatalysis by this nitride oxide if its use in a water splitting reaction systems is to be realized.

Conclusion

Spinel phases of $Zn_xTiO_yN_z$ were obtained by nitriding an oxide precursor derived from a polymerized complex route under a 100 mL min^{-1} of NH_3 flow at 1023 K. Zn species occupied both tetrahedral and octahedral sites in the spinel structure, while Ti species were located preferentially at octahedral sites. The $Zn_xTiO_yN_z$ spinel was a metastable phase because of continuous volatilization of Zn during the nitridation. It is found that Zn species at the octahedral sites of the $Zn_xTiO_yN_z$ spinel volatilized in preference to those at the tetrahedral sites. Indirect bandgap energy of the $Zn_xTiO_yN_z$ spinel was estimated to be 2.3 eV after sufficient nitridation. Incorporation of N^{3-} anions into the spinel structure was responsible for the bandgap narrowing. However, severe nitridation caused collapse of the spinel structure of $Zn_xTiO_yN_z$ due to a reduction in Zn content rather than an increase in N content and bandgap narrowing. The $Zn_xTiO_yN_z$ spinel exhibited photocatalytic activity for H_2 and O_2 evolution reactions under visible light irradiation ($\lambda > 420$ nm) in the presence of sacrificial reagents. Optimally prepared $Zn_xTiO_yN_z$ showed an apparent quantum efficiency of 1.0% for the O_2 evolution reaction, while an apparent quantum efficiency of less than 0.01% for the H_2 evolution reaction.

This work was supported by Research and Development in a New Interdisciplinary Field Based on Nanotechnology and Materials Science Program of the Ministry of Education, Culture, Sports, Science and Technology of Japan (MEXT) and the Global Centre of Excellence (GCOE) Program for Chemistry Innovation.

References

1 K. Sayama, K. Mukasa, R. Abe, Y. Abe, H. Arakawa, *J. Photochem. Photobiol., A* **2002**, *148*, 71.
2 H. Kato, M. Hori, R. Konta, Y. Shimodaira, A. Kudo, *Chem. Lett.* **2004**, *33*, 1348.
3 K. Maeda, K. Teramura, D. Lu, T. Takata, N. Saito, Y. Inoue, K. Domen, *Nature* **2006**, *440*, 295.
4 Y. Lee, K. Teramura, M. Hara, K. Domen, *Chem. Mater.* **2007**, *19*, 2120.
5 M. Kitano, M. Takeuchi, M. Matsuoka, J. Thomas, M. Anpo, *Catal. Today* **2007**, *120*, 133.
6 M. Higashi, R. Abe, K. Teramura, T. Takata, B. Ohtani, K. Domen, *Chem. Phys. Lett.* **2008**, *452*, 120.
7 H. Kato, A. Kudo, *J. Phys. Chem. B* **2001**, *105*, 4285.
8 T. Takata, Y. Furumi, K. Shinohara, A. Tanaka, M. Hara, J. N. Kondo, K. Domen, *Chem. Mater.* **1997**, *9*, 1063.
9 S. Ikeda, M. Hara, J. N. Kondo, K. Domen, *Chem. Mater.* **1998**, *10*, 72.
10 K. Maeda, K. Teramura, T. Takata, M. Hara, N. Saito, K. Toda, Y. Inoue, H. Kobayashi, K. Domen, *J. Phys. Chem. B* **2005**, *109*, 20504.
11 K. Maeda, K. Teramura, N. Saito, Y. Inoue, K. Domen, *Bull. Chem. Soc. Jpn.* **2007**, *80*, 1004.
12 Y. Lee, H. Terashima, Y. Shimodaira, K. Teramura, M. Hara, H. Kobayashi, K. Domen, M. Yashima, *J. Phys. Chem. C* **2007**, *111*, 1042.
13 S. Ikeda, T. Itani, K. Nango, M. Matsumura, *Catal. Lett.* **2004**, *98*, 229.
14 S. Ikeda, M. Fubuki, Y. K. Takahana, M. Matsumura, *Appl. Catal., A* **2006**, *300*, 186.
15 Z. Lei, W. You, M. Liu, G. Zhou, T. Takata, M. Hara, K. Domen, C. Li, *Chem. Commun.* **2003**, 2142.
16 K. Ikarashi, J. Sato, H. Kobayashi, N. Saito, H. Nishiyama, Y. Inoue, *J. Phys. Chem. B* **2002**, *106*, 9048.
17 F. Grasset, L. Spanhel, S. Ababou-Girard, *Superlattices Microstruct.* **2005**, *38*, 300.
18 F. Grasset, G. Starukh, L. Spanhel, S. Ababou-Girard, D.-S. Su, A. Klein, *Adv. Mater.* **2005**, *17*, 294.
19 D. Berthebaud, F. Grasset, V. Allegret-Maret, S. Ababou-Girard, S. Pechev, *J. Phys. Chem. C* **2007**, *111*, 7883.
20 T. Hisatomi, K. Hasegawa, K. Teramura, T. Takata, M. Hara, K. Domen, *Chem. Lett.* **2007**, *36*, 558.
21 D. E. Scaife, *Sol. Energy* **1980**, *25*, 41.
22 J. A. Schottenfeld, A. J. Benesi, P. W. Stephens, G. Chen, P. C. Eklund, T. E. Mallouk, *J. Solid State Chem.* **2005**, *178*, 2313.
23 A. Kasahara, K. Nukumizu, G. Hitoki, T. Takata, J. N. Kondo, M. Hara, H. Kobayashi, K. Domen, *J. Phys. Chem. A* **2002**, *106*, 6750.
24 R. D. Shannon, *Acta Crystallogr., Sect. A* **1976**, *32*, 751.
25 S. F. Bartram, R. A. Slepetys, *J. Am. Ceram. Soc.* **1961**, *44*, 493.
26 T. Yamamoto, *Adv. X-Ray Chem. Anal., Jpn.* **2007**, *38*, 45.
27 C. H. Shin, G. Bugli, G. Djega-Mariadassou, *J. Solid State Chem.* **1991**, *95*, 145.
28 F. Farges, G. E. Brown, Jr., J. J. Rehr, *Phys. Rev. B* **1997**, *56*, 1809.
29 R. L. Millard, R. C. Peterson, B. K. Hunter, *Am. Mineral.* **1995**, *80*, 885.
30 A. Navrotsky, O. J. Kleppa, *J. Inorg. Nucl. Chem.* **1967**, *29*, 2701.
31 M. A. Arillo, M. L. López, C. Pico, M. L. Veiga, A. Jiménez-López, E. Rodríguez-Castellón, *J. Alloys Compd.* **2001**, *317–318*, 160.
32 G. Schön, *J. Electron Spectrosc. Relat. Phenom.* **1973**, *2*, 75.
33 L. Yin, T. Tsang, I. Adler, E. Yellin, *J. Appl. Phys.* **1972**, *43*, 3464.
34 M. Futsuhara, K. Yoshioka, O. Takai, *Thin Solid Films* **1998**, *322*, 274.
35 C. D. Wagner, A. Joshi, *J. Electron Spectrosc. Relat. Phenom.* **1988**, *47*, 283.
36 N. D. Shinn, K.-L. Tsang, *J. Vac. Sci. Technol., A* **1991**, *9*, 1558.
37 F. Tessier, R. Assabaa, R. Marchand, *J. Alloys Compd.* **1997**, *262–263*, 512.
38 L. Le Gendre, R. Marchand, Y. Laurent, *J. Eur. Ceram. Soc.* **1997**, *17*, 1813.
39 M. Jansen, H. P. Letschert, *Nature* **2000**, *404*, 980.
40 W.-J. Chun, A. Ishikawa, H. Fujisawa, T. Takata, J. N. Kondo, M. Hara, M. Kawai, Y. Matsumoto, K. Domen, *J. Phys. Chem. B* **2003**, *107*, 1798.
41 A. Kasahara, K. Nukumizu, T. Takata, J. N. Kondo, M. Hara, H. Kobayashi, K. Domen, *J. Phys. Chem. B* **2003**, *107*, 791.
42 K. Maeda, Y. Shimodaira, B. Lee, K. Teramura, D. Lu, H. Kobayashi, K. Domen, *J. Phys. Chem. C* **2007**, *111*, 18264.
43 Y.-I. Kim, P. M. Woodward, K. Z. Baba-Kishi, C. W. Tai, *Chem. Mater.* **2004**, *16*, 1267.

44 K. Maeda, H. Hashiguchi, H. Masuda, R. Abe, K. Domen, *J. Phys. Chem. C* **2008**, *112*, 3447.
45 B. Ohtani, Y. Okugawa, S. Nishimoto, T. Kagiya, *J. Phys. Chem.* **1987**, *91*, 3550.
46 S. Sato, J. M. White, *J. Am. Chem. Soc.* **1980**, *102*, 7206.
47 M. Hara, T. Takata, J. N. Kondo, K. Domen, *Catal. Today* **2004**, *90*, 313.